

高介電係數介電質與金屬閘極製程技術應用在

金屬-氧化層-氮化層-氧化層-矽結構之非揮發性記憶體

研究生：賴軍宏

指導教授：荊鳳德教授

國立交通大學

電子工程學系暨電子研究所

摘要

近年來，在半導體產業中，記憶體元件的發展已成為另一主流。其中，屬於非揮發性型態的快閃式記憶體因其具有高密度特性、良好的資料保存能力和重複抹寫功能而被廣泛地使用在個人行動電子產品，例如手機或數位相機。隨著這些電子產品的普及化，對快閃式記憶體的需求也快速增加。因此，快閃式記憶體的發展和技術已成為重要的研究之一。

隨著元件尺寸持續縮微，快閃式記憶體主要的製程技術關鍵為其具有導電性的多晶矽浮停閘。基於非揮發性記憶體基本的需求，以多晶矽材料當作電荷儲存層的快閃式記憶體需要厚度至少約6-7奈米的穿遂氧化層來防止儲存電荷遺失以增加資料儲存能力。其主要原因為反覆的編碼和抹除過程將會對穿遂氧化層造成應力而產生缺陷，這些缺陷可能形成漏電路徑而導致多晶矽全面性的漏電。然而，較厚的穿遂氧化層不僅需要較大的操作電壓也增加元件製程縮微的困難度。為了解決此問題，多晶矽材料將被氮化矽所取代。由氮化矽電荷儲存層所形成的多晶矽或金屬閘極-氧化矽-氮化矽-氧化矽-矽結構記憶體元件可以解決平面微

縮的問題且同時具有良好電荷儲存能力、低工作電壓特性和符合目前互補式金氧半場效電晶體元件的製程，因此已開始受到大家的關注。

在此論文中，我們使用全新的高介電係數介電質材料氮化鋁（介電係數約 10）和氧化鈣鋁（介電係數約 17）分別取代傳統的氮化矽電荷捕獲層及氧化矽阻擋層。高介電係數介電質的使用，不僅可以有效降低操作電壓，同時也可以將電壓有效的跨在薄二氧化矽穿隧層以增加編碼和抹寫速度。此外，應用具高功函數的金屬閘極氧化銱替代傳統多晶矽閘極可以防止在抹除狀態時電荷從閘極端注入並增加抹除效率。此非揮發性記憶體元件展現出非常大的記憶視窗（3.7 伏）、快速（100 微秒）、低電壓（13 伏）操作和良好的資料儲存特性。

為了更進一步的降低記憶體元件操作電壓使其達到嵌入式單一晶片系統的應用。我們使用具有更高介電係數的介電質材料-氮氧化鈣（介電係數約 22）當作元件的電荷捕獲層。此氮氧化鈣記憶體元件展現出快速（100 微秒）和超低電壓（8 伏）操作特性。同時具有良好的資料儲存特性。另外，設計一簡單的電路可將此記憶體元件之操作電壓減少一半以達到單一晶片系統的應用。

Process and Technology for High- κ Metal Gate MONOS Structured Non-volatile Memory

Student: C. H. Lai

Advisor: Dr. Albert Chin

**Department of Electronics Engineering
& Institute of Electronics
National Chiao Tung University**

Abstract

Recently, the Flash memory is commonly used in portable electronic products, such as cell phone, MP3 player and USB Flash. However, with the increase in requirements for products, the technology and process must be still improved.

The key issue for poly-Si floating gate non-volatile memory is the electrically conductive charge storage layer, where the programmed electrons will leak out through the single oxide defect. Such oxide defects are generated by the program and erase stress operation. In order to maintain the data retention, the thick tunnel oxide (6-7 nm) is required. That is opposite to the VLSI scaling trend. In addition, the memory device with thick tunnel oxide requires a higher operation voltage. To overcome this problem, the conductive poly-Si is replaced by discrete trapping nitride to form the [poly-Si or metal gate]-SiO₂-SiN-SiO₂-Si SONOS or MONOS memory. The isolated charges stored in discrete traps can prevent complete charge leakage. Therefore, a thinner tunnel oxide can be used. This in turn yields lower voltage and

faster speed for program and erase.

In this dissertation, we demonstrated a low voltage, fast speed and good data retention MONOS memory device with high work function IrO_x metal gate, novel high- κ AlN trapping layer and HfAlO blocking layer. At 13 V and 100 μs program and -13 V 100 μs erase, we found a large threshold voltage shift (ΔV_{th}) of 3.7 V that extrapolated to 1.9 V for 10-year retention at 85°C. This 100 μs speed, low operation voltage of 12-13 V, withstand above 10 k cycles and 1.9 V 10-year memory retention window at 85°C meet all the non-volatile memory requirements simultaneously.

Using the same concept, we further provide the TaN-HfAlO-HfON-SiO₂-Si MONOS device to operate at only 8 V under faster 100 μs . Such low P/E voltage is achieved by using novel HfON trapping layer with very high κ of 22 beyond AlN ($\kappa \sim 10$). Under fast 100 μs at ± 8 V for P/E, the device exhibits a large initial ΔV_{th} (memory window) of 2.5 V and the 10-years extrapolated retention window of 1.0 V at even 125°C. Using a simple voltage inverter circuit, the P/E voltage can further be reduced to nearly half: by applying 4.5 V and -3.5 V for the same ± 8 V gate-channel bias. This is useful for embedded SoC under a single 5 V voltage source.

Acknowledgement

First, I would like to thank my advisor Prof. Albert Chin for his fruitful discussion and illuminative comment. I am also grateful to all ED633 group members, Dr. C. Y. Lin, Dr. S. B. Chen, Dr. M. Y. Yang, Dr. C. H. Huang, Dr. D. S. Yu, Dr. C. C. Chen, Dr. H. L. Kao, C. H. Wu, B. F. Hung, K. C. Chiang, Terry Wang, Z. W. Lin and W. L. Huang, for their enthusiastic assistance and cooperation. Moreover, I thank for my girl friend Miss Chan, Hui-Ting. Finally, I deeply appreciate my family and parents' endless encouragement and spiritual support. Without them, I can't finish this dissertation.



Contents

Abstract (in Chinese)	i
Abstract (in English)	iii
Acknowledgement	v
Contents	vi
Figure Captions	viii
Table Captions	xvi

Chapter 1 Introduction

1.1 Motivation to study high- κ dielectrics.....	1
1.2 Motivation to study metal gate.....	3
1.3 Motivation to study MONOS memory.....	5
1.4 The measurement of the devices.....	6
1.5 Innovation and contribution.....	7

Chapter 2 A Novel Program-erasable High- κ AlN/Si MIS Capacitor

2.1 Introduction.....	23
2.2 Experimental.....	24
2.3 Results and discussion.....	24
2.4 Conclusion.....	27

Chapter 3 The Tunable and Program-erasable RF MIS Capacitor with Long Tuning Memory

3.1 Introduction.....	41
3.2 Experimental.....	42
3.3 Results and discussion.....	43
3.4 Conclusion.....	46

Chapter 4 Novel SiO₂/AlN/HfAlO/IrO_x Memory with Fast Erase, Large ΔV_{th} and Good Retention

4.1 Introduction.....56
4.2 Experimental.....57
4.3 Results and discussion.....58
4.4 Conclusion.....60

Chapter 5 Very Low Voltage SiO₂/HfON/HfAlO/TaN Memory with Fast Speed and Good Retention

5.1 Introduction.....76
5.2 Experimental.....77
5.3 Results and discussion.....78
5.4 Conclusion.....84

Chapter 6 Conclusion.....102

References.....104

Vita.....127

Publication List.....128

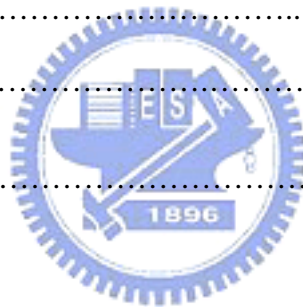


Figure Caption

Chapter 1 Introduction

Fig. 1-1 The evolution of MOS technology requirement.

Fig. 1-2 The κ value of high- κ materials.

Fig. 1-3 The band offset of popular high- κ materials.

Fig. 1-4 The advantages and requirements of metal gate technology.

Fig. 1-5 The values of work function for different metal materials.

Fig. 1-6 The advantages and functions of non-volatile Flash memory.

Fig. 1-7 Hot carrier problems in the electrically conductive poly-Si floating gate

Flash memory.

Fig. 1-8 The cross section of metal [gate/poly-Si]-SiO₂-Si₃N₄-SiO₂-Si memory.

Fig. 1-9 The requirements for SONOS memory from ITRS.

Fig. 1-10 The measurement set-up for S-parameter.

Fig. 1-11 The summary and structure of this dissertation.

Chapter 2 A Novel Program-erasable High- κ AlN/Si MIS Capacitor

Fig. 2-1 Cross section view of novel program-erasable high- κ AlN MIS capacitor.

Fig. 2-2 The measured C-V hysteresis of 16 nm AlN/Si MIS capacitors after (a) as-deposited and (b) 400°C 5 min PDA process.

Fig. 2-3 The XRD measurement of as-deposited and 400°C PDA AlN dielectrics.

The high- κ AlN dielectrics are amorphous after 400°C and 20 min annealing.

Fig. 2-4 The high- κ AlN single layer MIS capacitor behaves program characteristics under 4 V~11 V for 1 ms.

Fig. 2-5 (a) The measured C-V characteristics, and (b) the threshold V_{th} as a function of the duration of the applied voltage, for a single layer high- κ AlN/Si MIS capacitor. The program and erase properties were obtained by applying voltages from ± 2 V to ± 4 V respectively.

Fig. 2-6 C-V characteristics of an Al/Si₃N₄/Si MIS capacitor. In contrast, a small C-V shift was shown after applying voltages of +4 and -4 V, which suggests shallower trap energy or lower trap density in the Si₃N₄ MIS device.

Fig. 2-7 The measured C-V characteristics of high- κ single layer Al₂O₃ MIS capacitors. Continuously increasing V_{th} is observed and can not be erased by negative voltage.

Fig. 2-8 The measured C-V characteristics of high- κ single layer AlON MIS capacitors. Continuously increasing V_{th} is observed at negative voltage without the erase function.

Fig. 2-9 The measured J-V characteristics of AlN capacitor. The fast decreasing slope may be due to charge trapping in AlN and decrease the subsequent

carriers' tunnel rate.

Fig. 2-10 The schematic band diagram of the metal-gate/high- κ dielectric/Si MIS capacitor.

Fig. 2-11 The schematic band diagram of the Al metal gate/high- κ AlN/Si MIS capacitor.

Fig. 2-12 (a) The C-V characteristics of an AlN MIS capacitor used for retention, measured from 10 s to 10000 s after removing the 1 ms +4 V program or -4 V erase voltage; (b) the threshold V_{th} as a function of retention time, derived from (a).

Fig. 2-13 The cycling property of Al/AlN/Si MIS capacitor.



Chapter 3 The Tunable and Program-erasable RF MIS Capacitor with Long Time Tuning Memory

Fig. 3-1 The application of a program-erasable high- κ tunable capacitor for (a) VCO and (b) RF amplifier. The tuning memory of the device can greatly simplify the VCO by eliminating an external voltage bias circuit and reducing the design turn-around time that may involve correcting the impedance mismatch in I/O LC networks of an RF amplifier.

Fig. 3-2 (a) Cross section and (b) top cell view of the RF AlN MIS capacitors.

Fig. 3-3 Measured C-V characteristics of a high- κ AlN MIS capacitor. A large

tuning range can be obtained in these high density capacitors using a high- κ gate dielectric. The shift of V_{FB} in the C-V curves is achieved by $+V_g$ and $-V_g$ for applied program and erase voltages, respectively.

Fig. 3-4 The measured C-V characteristics of an AlN MIS capacitor after a + 4 V program or a -4 V erase for 1 ms. The retention property was obtained by measuring the C-V, after removing the program or erase voltage, for 10 s to 10,000 s.

Fig. 3-5 The retention characteristics of $+V_{th}$ and $-V_{th}$ from the C-V curves in Fig. 4 for an AlN MIS capacitor programmed or erased at +4 V or -4 V for 1 ms. Excellent memory characteristics are shown, such as the small V_{th} variation and extrapolated long memory time.

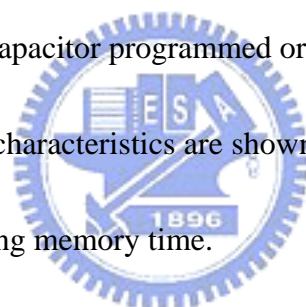


Fig. 3-6 The equivalent circuit model for an AlN capacitor simulation in the RF regime.

Fig. 3-7 The measured and simulated S-parameters of program-erasable AlN MIS capacitors.

Fig. 3-8 The frequency-dependent capacitance for the program-erasable AlN MIS capacitor.

Fig. 3-9 The Q-factor of a $4.8 \text{ fF}/\mu\text{m}^2$ AlN MIS capacitor as a function of frequency.

Chapter 4 Novel $\text{SiO}_2/\text{AlN}/\text{HfAlO}/\text{IrO}_x$ Memory with Fast Speed,

Large ΔV_{th} and Good Retention

Fig. 4-1 The cross-section view of Si/SiO₂/AlN/HfAlO/IrO_x MONOS memory device.

Fig. 4-2 The J-V characteristics of Ir/IrO₂ high- κ metal gate PMOS.

Fig. 4-3 The SIMS measurement of IrO_x film.

Fig. 4-4 The band diagram of an IrO_x-HfAlO-AlN-SiO₂-Si MONOS device in the erase state. The AlN has a strong trapping capability and the high work-function IrO_x metal gate decreases the charge injection into the thin HfAlO blocking layer.

Fig. 4-5 J_g - V_g curves of MONOS memory with 12 nm and 16 nm AlN at 25 and 85°C. The J_g is 1 order of magnitude lower than the data from [4.6] due to higher work function of IrO_x.

Fig. 4-6 C-V hysteresis curves of MONOS capacitor with 16 nm AlN for various V_g . The capacitance density increases to 3.5 fF/ μm^2 for 12 nm AlN device.

Fig. 4-7 The measured I_d - V_g characteristics of IrO_x-HfAlO-12 nm AlN-SiO₂-Si MONOS device.

Fig. 4-8 The measured (a) program and (b) erase characteristics from I_d - V_g for 16 nm AlN MONOS devices 10 μm gate length. The device was initially programmed at 13 V for 100 μs .

Fig. 4-9 The measured (a) program and (b) erase characteristics from I_d - V_g for 12 nm AlN MONOS devices 10 μ m gate length. The device was initially programmed at 13 V for 100 μ s.

Fig. 4-10 Retention of MONOS devices with 16 nm AlN at 25°C. The P/E decay rates are only 72/22 mV/dec.

Fig. 4-11 Retention of MONOS devices with 12nm AlN at 25°C. The P/E decay rates are 92/49 mV/dec.

Fig. 4-12 Retention of MONOS devices with 12 nm and 16 nm AlN at 85°C. The P/E decay rates are 120/64 mV/dec.

Fig. 4-13 Endurance of MONOS memory with (a) 16 nm and (b) 12 nm AlN at 85°C. High ΔV_{th} can be maintain up to 10^4 or 10^5 P/E.

Fig. 4-14 Retention of 10 k P/E-cycled MONOS devices with (a) 16 nm and (b) 12 nm AlN at 85°C. Large ΔV_{th} of 1.6 and 2.7 V are still obtained in 12 nm AlN MONOS device.

Chapter 5 Very Low Voltage SiO₂/HfON/HfAlO/TaN Memory with Fast Speed and Good Retention

Fig. 5-1 The structure of TaN-HfAlO-HfON-SiO₂-Si MONOS memory device.

Fig. 5-2 The SIMS profiles of oxygen and nitrogen in the HfO₂ and HfON layers.

Fig. 5-3 X-ray photoelectron survey spectra of the HfON high-κ dielectric.

Fig. 5-4 XPS characteristics of (a) Hf_{4f} spectra and (b) N_{1s} spectra of HfON and control HfO₂ dielectrics.

Fig. 5-5 (a) Energy band diagram of TaN-HfAlO-[trapping layer]-SiO₂-Si MONOS device with different Si₃N₄, AlN or HfON high-κ trapping layer; (b) energy band diagram of MONOS under erase function.

Fig. 5-6 C-V hysteresis curves of HfON MONOS capacitor. Very high capacitance density ~4fF/μm² is obtained.

Fig. 5-7 The J_g-V_g characteristics of TaN-HfAlO-HfON-SiO₂-Si MONOS under erase at 25-125°C.



Fig. 5-8 The I_d-V_g and gm curves of HfON MONOS transistors.

Fig. 5-9 The P/E characteristics of HfON MONOS device. (a) The measured program characteristics from I_d-V_g of transistors (b) The measured erase characteristics from I_d-V_g of transistors.

Fig. 5-10 Measured and TMA simulated J-V curves. The erase speed also depends on the hole injection from the Si channel.

Fig. 5-11 The diode-clamp circuit to generate negative -3.5 V from supplied 4.5 V voltage source using TSMC 0.18 μm library.

Fig. 5-12 Endurance characteristics of TaN-HfAlO-HfON-SiO₂-Si MONOS device.

The memory window is almost constant until 10 k P/E cycles with only 12% degradation.

Fig. 5-13 Retention characteristics of fresh TaN-HfAlO-HfON-SiO₂-Si MONOS devices at (a) room temperature and (b) elevated temperature.

Fig. 5-14 Retention characteristics of 10³ P/E cycled MONOS devices.

Fig. 5-15 The band diagram of TaN-HfAlO-HfON-SiO₂-Si MONOS memory device in retention mode.



Table Caption

Chapter 4 Novel SiO₂/AlN/HfAlO/IrO_x Memory with Fast Speed, Large ΔV_{th} and Good Retention

Table 4-1 Comparisons of P/E speed, ΔV_{th} window (extrapolated for 85°C 10-years retention), retention decay rate and endurance.

Chapter 5 Very Low Voltage SiO₂/HfON/HfAlO/TaN Memory with Fast Speed and Good Retention

Table 5-1 Comparisons of P/E condition, ΔV_{th} and reliability of TaN-HfAlO-HfON-SiO₂-Si MONOS memory with published data.

Table 5-2 The device parameters used for TMA simulation.

